Traffic 2006; **7:** 1628–1642
Blackwell Munksgaard

doi: 10.1111/j.1600-0854.2006.00496.x

Dynamic Organization of the Actin Cytoskeleton During Meiosis and Spore Formation in Budding Yeast

Christof Taxis, Celine Maeder, Simone Reber[1], Nicole Rathfelder, Kota Miura, Klaus Greger, Ernst H. K. Stelzer and Michael Knop*

Cell Biology and Biophysics Unit, EMBL, Meyerhofstr. 1, Heidelberg 69117, Germany
[1]Current address: Universität Heidelberg, ZMBH, Im Neuenheimer Feld 282, Heidelberg 69120, Germany
**Corresponding author: Michael Knop, knop@embl.de*

During sporulation in *Saccharomyces cerevisiae*, the four daughter cells (spores) are formed inside the boundaries of the mother cell. Here, we investigated the dynamics of spore assembly and the actin cytoskeleton during this process, as well as the requirements for filamentous actin during the different steps of spore formation. We found no evidence for a polarized actin cytoskeleton during sporulation. Instead, a highly dynamic network of non-polarized actin cables is present underneath the plasma membrane of the mother cell. We found that a fraction of prospore membrane (PSM) precursors are transported along the actin cables. The velocity of PSM precursors is diminished if Myo2p or Tpm1/2p function is impaired. Filamentous actin is not essential for meiotic progression, for shaping of the PSMs or for post-meiotic cytokinesis. However, actin is essential for spore wall formation. This requires the function of the Arp2/3p complex and involves large carbohydrate-rich compartments, which may be chitosome analogous structures.

Key words: actin, cell polarity, meiosis, sporulation, vesicle movement, yeast

Received 3 March 2006; revised and accepted for publication 6 September 2006

Mitotic cell division in baker's yeast *Saccharomyces cerevisiae* is accompanied by formation of a bud, which is connected to the mother cell by the bud neck. Subsequent division processes involve polarized growth of the plasma membrane in the bud and sequestration of cytoplasmic contents, including organelles and half of the nucleus into the daughter cell (1,2). A different morphogenetic programme, called sporulation, is performed during the meiotic cell divisions. The formation of the four meiotic progeny, the spores, occurs entirely in the cytoplasm of the mother cell (3–5).

The new plasma membranes are formed from the so-called prospore membrane (PSM) precursors. The PSM precursors assemble at the spindle pole bodies (SPBs) in meiosis II to form the PSMs (6,7). Secretory vesicles and the exocyst are redirected towards the SPB and initiate PSM formation by homotypic vesicle fusion (8–10). Then the four PSMs grow out through the cytoplasm around the lobes of the nucleus. At the end of the meiotic divisions, after fission of the nuclear envelope, the PSMs close and each new compartment contains a haploid set of chromatids.

Two structures specific for this process have been described: the meiotic plaque (MP) and the leading edge protein (LEP) coat [for a review, see (3)]. The MP of the SPBs has been demonstrated to be required for the initiation of membrane formation. It consists of at least three essential proteins (Mpc54p, Mpc70p, Spo74p), and one protein (Ady4p) with auxiliary function (7,11,12). In the absence of MPs, few PSM precursors bind to the SPBs, the others remain in the cytoplasm. These precursor structures are characterized by their content of the proteins Ssp1p, Ady3p and Don1p. Many precursor structures contain the t-SNAREs Sso1p and Sso2p as well (7,13). The proteins Ssp1, Ady3p and Don1p relocalize to the leading edge of the growing PSM after fusion of the precursor structures at the SPB. These proteins form the so-called LEP coat (13,14).

The faithful and simultaneous completion of four new membrane systems requires the presence of regulatory mechanisms that ensure the concomitant initiation of membrane formation at all four SPBs, the equal distribution of subsequent membranes to the four growing membrane systems, redirection of secretory vesicles towards the PSMs and the simultaneous closure of all membranes upon exit of meiosis II and concomitant cytokinesis.

Afterwards, the prospore is enclosed by the PSM, which consists of two membrane bilayers on top of each other. Subsequently, maturation of the spore walls occurs through deposition of the different layers of spore wall material between the two membrane bilayers (15–18).

Here, we describe a detailed dissection of the assembly of the PSMs and spores with regards to the role of the actin cytoskeleton in this process. We found that actin is essential for maturation of the spore wall, but not for the assembly, shaping and closure of the PSMs. We performed a detailed analysis of the dynamic organization of actin cables and actin patches during progression of meiosis and sporulation and investigated how these structures contribute to the different steps of spore formation.

Our results reveal a completely different organization of these processes during meiotic cell differentiation as compared with polarized cell division during vegetative growth. No evidence for a polarization of the actin cytoskeleton was detected. Actin-cable-mediated PSM precursor transport occurs during meiotic cell differentiation, but is not essential for spore formation. Instead, we found an essential requirement for Arp2p during spore wall maturation. Arp2 is a key subunit of the Arp2/3p complex required for the integrity and mobility of actin patches (19).

Results

Three stages of prospore membrane assembly

Assembly of the spores during meiosis and sporulation in yeast occurs within the plasma membrane of the mother cell. To follow the dynamics of PSM assembly, we used green fluorescent protein (GFP) fused to Don1p as a marker for PSM precursors and the PSMs themselves (7). We performed live cell imaging to analyse the dynamics of the different steps of this process. This revealed that three different stages could be distinguished: assembly, growth and closure of the PSMs (Figure 1A, B; Movies S1, S2).

Initially, precursor structures can be detected in the SK1 yeast background at around 4 h after induction of sporulation, when the first cells in the population start to enter meiosis I. At this stage, they appear as dot-like structures that are scattered throughout the cell (Figure 1A; 0–12′). The number of structures varies from cell to cell and falls in the range of approximately 10–25. The number of precursors then gradually decreases, while four bright signals become apparent. These signals label the area of the SPBs, where PSM assembly takes place (Figure 1A; 12′). Then the four bright dots each form a donut-like structure, indicative of the assembly of domed PSMs (Figure 1A; 18′). Don1p–GFP localizes to the leading edge of the membrane during this phase (7).

During the next stage (Figure 1B), the PSMs grow around the nuclear lobes (7, 13). The size of the Don1p–GFP 'donuts' remains constant throughout this period (Figure 1B, 0–42′). Finally, the donuts start to shrink in diameter, until they disappear completely, which indicates closure of the PSMs (Figure 1B, 42–48′). The period of shrinkage and closure of the PSMs usually lasts 5–9 min. In all cases we investigated ($n > 50$), shrinkage occurred simultaneously for all donuts present in one cell. Often, we observed a faint staining of four dots inside the cell (Figure 1B, arrow heads in frame 54′). These may be Don1p–GFP localizing at the SPBs.

We distinguished two different types of precursors during the initial stages of PSM assembly. Static precursor structures were visible during the whole process of PSM assembly (Figure 1A, white arrows). Their signal became less bright during the assembly of the PSMs. In addition, highly dynamic precursor structures were found (Figure 1A, outlined arrow heads). To address the movements of these precursors in detail, we recorded shorter movies with a higher frame rate. The cells were imaged once every 4 seconds and these images were compiled into movies. Typically, 1–3 mobile precursors were visible in each 2 min movie. As shown by object tracking (Figure 1C), they changed their velocity very often. The precursors moved mostly for a short distance between the frames, but occasionally very fast movements could be observed. The fastest movements we recorded were in the range of 0.3–0.5 μm/second. In some cases, we saw that these mobile structures merged with less mobile precursors, which might be located at the SPBs (Figure 1C; Movies S3, S4).

Actin filaments are required for spore maturation but not for PSM assembly and formation of prospores

A polarized actin cytoskeleton is essential for mitotic cell division at several stages. Three steps can be distinguished morphologically: bud initiation, bud growth as well as shaping and closure of the bud-daughter connection during cytokinesis. These steps and their faithful progression require a polarized actin cytoskeleton (1,20). Equivalent steps can also be distinguished during PSM assembly and spore formation: the initiation of PSM formation, growth and shaping as well as closure of the PSM.

To address the requirement of actin during sporulation, we used Latrunculin A (Lat-A) treatment and sporulation time–course analysis with synchronously sporulating cells. Latrunculin A sequesters monomeric actin (21) and therefore depolymerizes actin filaments. Figure 2A depicts meiotic progression of cells undergoing synchronous sporulation. To analyse the consequences of actin depolymerization on sporulation in detail, we followed spore formation in aliquots of cells that were removed at different time-points during sporulation from the culture shown in Figure 2A. The cells were incubated with Lat-A and allowed to complete sporulation. Spore formation was investigated in comparison to control samples [treated with dimethyl sulphoxide (DMSO)] (Figure 2B). The fraction of spores present at the time-point of incubation with Lat-A was determined (Figure 2A). We verified that Lat-A treatment led to complete depolymerization of all filamentous actin structures throughout the entire incubation period (see *Materials and Methods*). The Lat-A treatment abolished sporulation completely when it was added prior to the meiotic divisions (before approximately 5 h). Addition of Lat-A also blocked spore formation at later stages because the number of spores present in the samples at the time-point of addition did not increase any further following addition of Lat-A. This suggests that Lat-A inhibits spore formation at a very late step, but does not exclude a potential block of other essential processes earlier in meiosis.

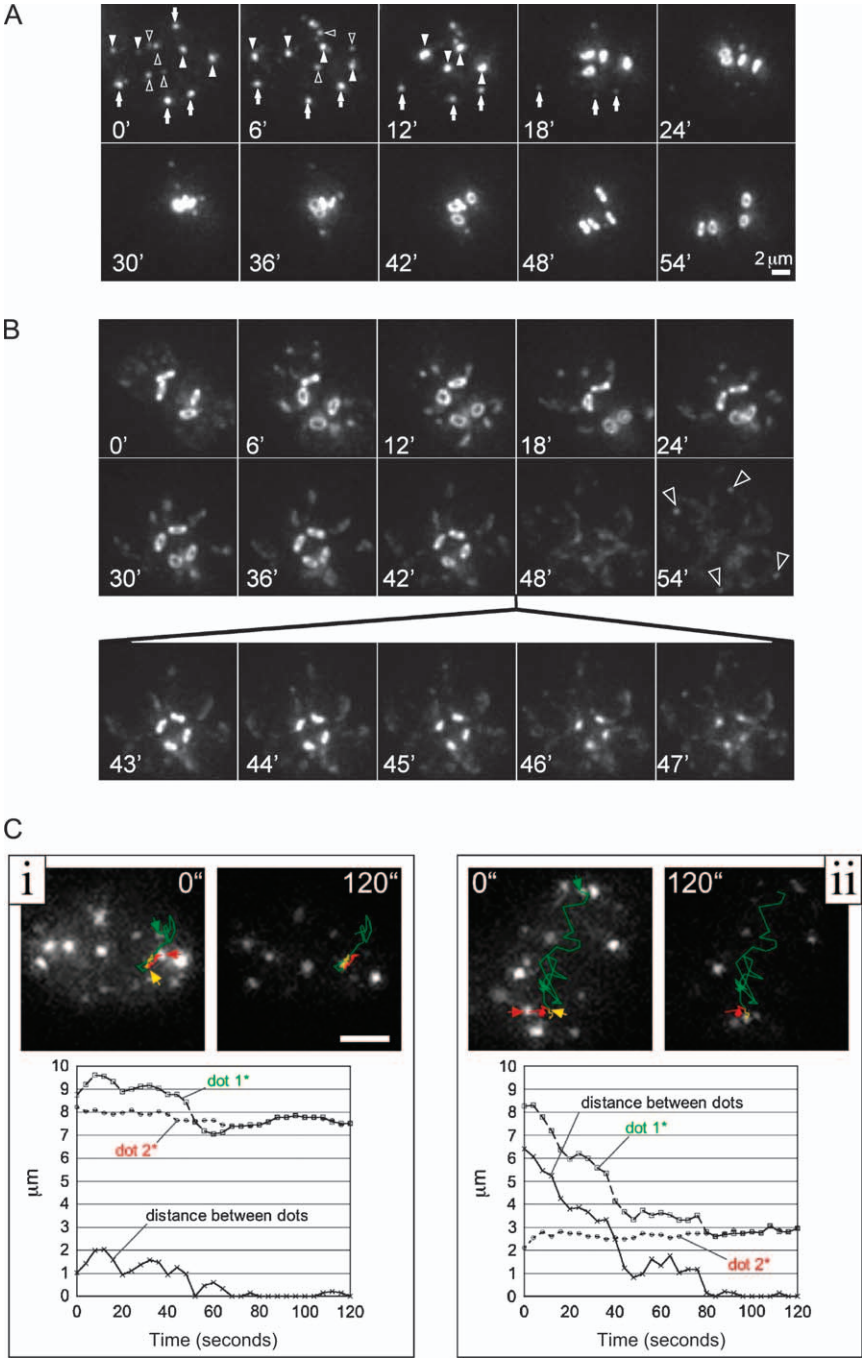

Figure 1: Live cell imaging of PSM assembly and precursor movements. A) Movie of a cell undergoing PSM assembly. Don1p–GFP was used as a specific marker for precursors and the leading edge of the PSM. White arrow heads: SPBs. Outlined arrow heads: fast moving precursors. Arrows: Immobile precursors. B) Closure of PSMs. Frames at intervals of 6 min are shown. Frames at intervals of 1 min are shown for the closure of the PSMs. Triangles point to Don1p–GFP signal localizing as a dot-like structure (one per prospore) after closure of the PSM. C) Track recording of fast precursor movements. Movies with frames (maximum projections) taken at intervals of 4 seconds were used for object tracking using METAMORPH™ software. The tracks of the observed precursors (green, fast moving precursor; red, slow moving precursor) are outlined on the first and the last picture of the sequences. (Full movies are shown as Movies S1–S4).

Investigation of the Don1p–GFP staining in Lat-A-treated cells revealed that the cells assembled prospores, which failed to build up mature spore walls (Figure 2C). Therefore, the spores cannot be detected by phase contrast microscopy. We followed the progression through meiosis and spore formation using Don1p–GFP as a marker to address whether Lat-A displays any noticeable effect on the assembly of the PSMs. This revealed that actin depolymerization did not cause an apparent delay in progression from early stages of PSM assembly to the formation of prospores (Figure 2D). Together, these results indicate a late and essential function of actin in spore maturation.

Filamentous actin is involved in precursor movements in meiosis II

We observed both fast-moving and static PSM precursors during early stages of PSM assembly (Figure 1A, C). Next, we asked whether polarized actin or actin-related transport contributes to these movements. We used a Don1p–GFP strain with additional deletions of genes encoding for

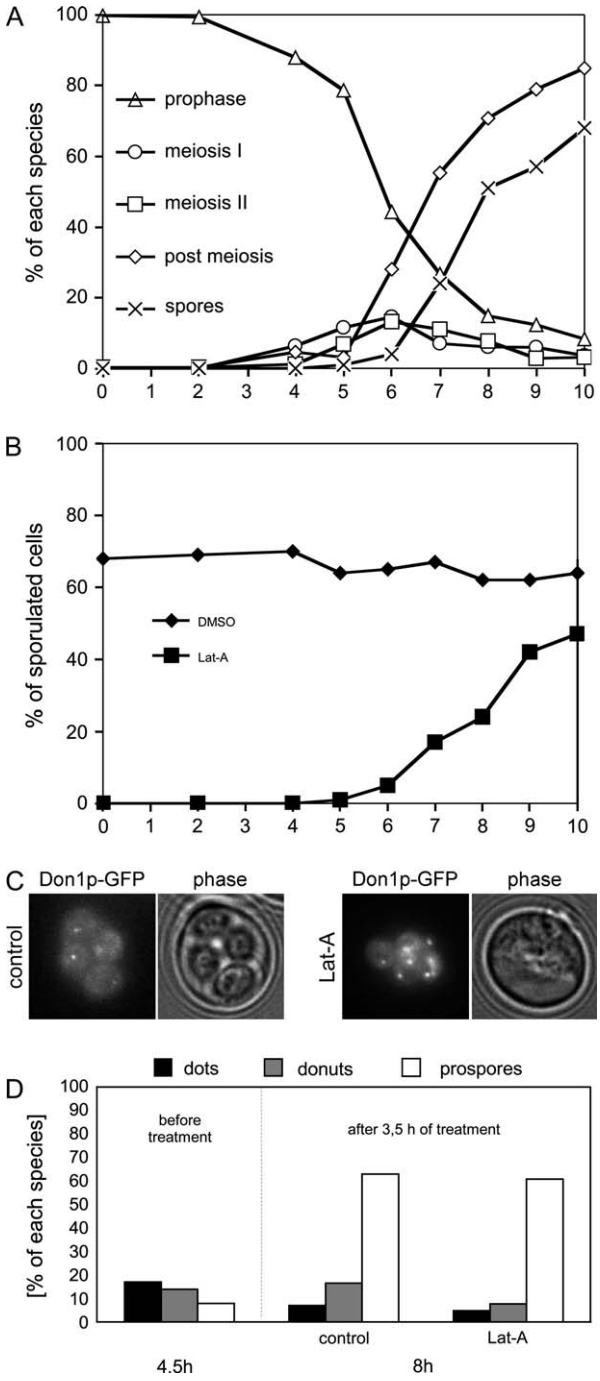

Figure 2: Filamentous actin is required for maturation of the spore wall. A) A wild-type cell culture undergoing synchronized sporulation. The composition of the culture at different time-points after induction of meiosis is shown. The different species were distinguished by Hoechst 33342 staining (prophase, meiosis I, meiosis II, post-meiosis) and phase contrast microscopy (spores). B) Samples of cells taken at the indicated time-points (hours) from the culture shown in (A) were incubated with DMSO or DMSO with Lat-A and allowed to complete sporulation (for another 16 h). The observed sporulation efficiency at the end of the incubation is plotted as a function of the time-point of Lat-A addition. One representative curve of three independent experiments is shown. At least 100 cells were examined at each time-point. C) Example of cells expressing Don1p–GFP and treated with DMSO or with DMSO and Lat-A for 6 h (added 4 h after induction of sporulation). Don1p–GFP fluorescence and phase contrast pictures were taken 10 h after induction of sporulation. D) Cells from a synchronously sporulationg culture were incubated with DMSO or Lat-A dissolved in DMSO. The composition of the culture was assessed using fluorescence microscopy for the presence of cells showing precursors, donuts and prospores before (4.5 h after induction of sporulation) and after treatment (8 h after induction of sporulation).

meiotic SPB components (Mpc54p and Mpc70p) to analyse PSM precursor movements. The absence of Mpc54p and Mpc70p prevents the assembly of PSMs and leads to homogenous populations of cells with accumulated precursors in the cytoplasm (7). Figure 3A shows the tracks of PSM precursors recorded in one cell. We observed highly mobile precursors in this strain as well (green track in Figure 3A; Movie S5). This suggests that the precursor movements are not dependent on the MP and therefore not on the meiotic function of the SPB. However, we did not observe merging precursors in this strain background. This supports the idea that the observed merging events in the wild-type recordings (Figure 1C) occur at SPBs. Quantitative measurement of the dynamics of all precursor movements in the presence and absence of Lat-A revealed that Lat-A treatment reduced the fraction of precursors with speeds >0.15 μm/4 seconds (Figure 3B). In addition, we measured the movements of other sporulation-specific structures. We analysed the movements of SPBs and LEP coats in wild-type cells expressing Don1p–GFP. This revealed that these structures also show dynamic movements that are actin dependent (Figure 3C). Together, our results suggest an active role of actin in generation of mobility of PSM-associated structures. However, actin-mediated movements of these structures (Figure 1C) appear to be non-essential because PSM assembly takes place in the Lat-A-treated cells (Figure 2D).

Two different strains with defects in actin-related transport were used to investigate whether fast precursor movements are caused by active transport along actin cables. The temperature-sensitive mutant *myo2-16* is impaired in vesicle transport along actin cables into the bud of vegetatively growing cells (22). In addition, we used a *Δtpm2 tpm1-2* temperature-sensitive mutant, in which actin cable stability is impaired at restrictive temperature (23). We noticed that this strain has a slow growth phenotype at 25°C in the SK-1 strain background used for sporulation analysis, suggesting a partial defect at permissive temperature. We investigated the movements of Don1p–GFP-labelled precursors in these cells during sporulation. We observed that the precursor mean velocity is reduced in the *myo2-16* cells at restrictive temperature and in the *Δtpm2 tpm1-2* mutants at both permissive and restrictive temperatures (Figure 3E, F). We tested the statistical significance of the differences in mean velocity by computation with the two-sample Student's *t*-test (24) at the 99.5% confidence

limit. At 25°C, the wild-type *MYO2* and the mutant *myo2-16* showed no difference in their mean velocities but at 34°C, the mean velocity of the mutant was siginificantly lower than that of the wild type (Figure 3E). In case of the tropomyosin mutants, the cells exhibited significantly lower velocity in both 25°C and 35°C as compared with the wild type (Figure 3F). This shows that the velocity of PSM precursors are significantly diminished in the mutants and suggests that active transport of precursors along actin cables takes place during the meiotic cell divisions.

Actin cables form a dynamic cage in the cell periphery during the meiotic cell divisions

The organization of actin cables and patches during the meiotic cell division have so far been investigated in fixed cells. The results demonstrate the presence of both, actin patches and actin cables in meiotic cells, but do not reveal any detail with respect to their spatio-temporal organization or their dynamics (25,26). To analyse actin cable dynamics in meiotic yeast, we used Abp140p, a previously established marker that labels actin cables (27,28). A homozygous diploid was generated containing 4GFP fused to Abp140p for live cell recordings. Comparison of mitotic and meiotic Abp140p–4GFP-expressing cells with wild-type cells using phalloidin labelling revealed no difference in the actin cytoskeleton in the two strains (Figure S1). It was reported that the Abp140p–1GFP construct labels not only actin cables but also actin patches in vegetative growing cells (28). However, we did not see Abp140p–4GFP localizing to actin patches in meiotic cells.

We recorded time-lapse movies of Abp140–4GFP cells undergoing sporulation. A Don1p–RFP fusion was used in these cells to simultaneously visualize the formation of the PSMs. Movies over periods of several hours revealed the presence of prominent actin cables throughout the stages of PSM assembly (Figure 4A; Movie S7). The appearance of the cables changed completely from frame to frame, indicating their dynamic behaviour. Furthermore, the actin cables are mainly located in the cell periphery underneath the plasma membrane throughout the meiotic cell division. Figure 4B shows a stereo picture of two 3D-reconstructed Abp140p–4GFP cells (for a 360° turn, see Movie S8). After PSM closure, actin cables can be seen inside the prospore as well (not shown). We also noticed that the overall appearance of the actin cables showed variations over time (see *Discussion*). In all the cases, no polarization of actin cables was apparent.

We next investigated the dynamics of actin cables using fast time-lapse recordings of only one plane in the periphery of the cells. The highly dynamic cables showed various types of interactions. Frequently, the cables showed lateral interactions with different parts of one cable interacting with parts of other cables. In roughly 50% of the cells, we observed cables combining with each other like a zipper during an observation period of 1 min (Figure 4C; Movie S9). In a few cases, bending of cables could also be observed (Figure 4D; Movie S10).

Next, we investigated whether actin cables slide along the plasma membrane. For this, we used the previously established method of low-dosage Lat-A incubation, which leads to a block of the repolymerization of cables, and thus enables the observation of actin cable movements, which are due to sliding and not tread milling (28). The average speeds of short cables observed in control cells and Lat-A-treated cells were similar and in the range of 0.3 μm/second (Figure 4E; Movies S11, S12). These speeds are comparable to the velocities of the fastest precursor structures (compare Figure 4E to Figure 1C).

We visualized actin cables together with PSM precursors (Don1p–RFP) to see whether PSM precursors are in proximity to actin cables. The recordings revealed that only a minority of precursors are co-localizing with actin cables. The precursors that did co-localize with actin cables were fast moving, indicating actin-cable-based transport. Figure 4F shows such an example. The precursor (indicated by a white arrow) is transported to the left (upper row) and then to the right (lower row). The figure shows 10 consecutive frames recorded at a rate of one frame every 2 seconds (movie provided as Movie S13). The fact that only a minority of the PSM precursors interact with the actin cables is in good agreement with the result (Figure 1) that only a small fraction of precursors exhibited fast movements during an observation period.

Taken together, our results demonstrate that actin cables form a cage-like, but highly dynamic network of interacting cables underneath the plasma membrane of sporulating cells, and that actin-based mobility is underlying fast but non-directed movements of precursors during PSM assembly.

Arp2p function is required for spore wall formation

To follow actin patches during sporulation, we used a GFP–Cap2p fusion protein as a marker for actin patches (23), and Don1p–RFP as a meiotic marker. We performed 3D live cell imaging to follow cells, as they progress through the meiotic divisions. We found that actin patches are equally distributed on the plasma membrane before meiosis II. During meiosis II, the patches are mostly concentrated in the part of the plasma membrane in the vicinity to the growing PSMs. After closure of the PSMs, the patches become visible in the interior of the cell, most probably on the membranes of the prospores. Occasionally, we observed actin patches in the interior of the cell during PSM assembly as well (Figure 5A; Movies S14, S15). These results indicate the continuous presence of actin patches throughout sporulation.

We observed that Lat-A treatment inhibited spore maturation (Figure 2A–C). To distinguish which types of actin organization (actin cables or actin patches) are required for

the essential function of actin in spore maturation, we investigated the sporulation ability of three mutants that interfere with the different types of actin organization. The mutant alleles we used were selected to have a restrictive temperature <35°C because meiosis is intrinsically temperature sensitive (29). In the SK-1 strain used for this study, the sporulation rate is reduced above 33°C and blocked above 35°C. We used an *arp2-1* mutant (30) to interfere with the functions of actin patches and a *Δtpm2 tpm1-2* mutant to disrupt actin cables (23). In addition, we analysed a *myo2-16* mutant, which is impaired in vesicular transport along actin cables (22).

Mutant and corresponding wild-type strains were sporulated at permissive and restrictive temperatures. The *myo2-16* and *Δtpm2 tpm1-2* strains did not show any difference in their sporulation efficiency when compared with the corresponding control cells (Figure 5B). This

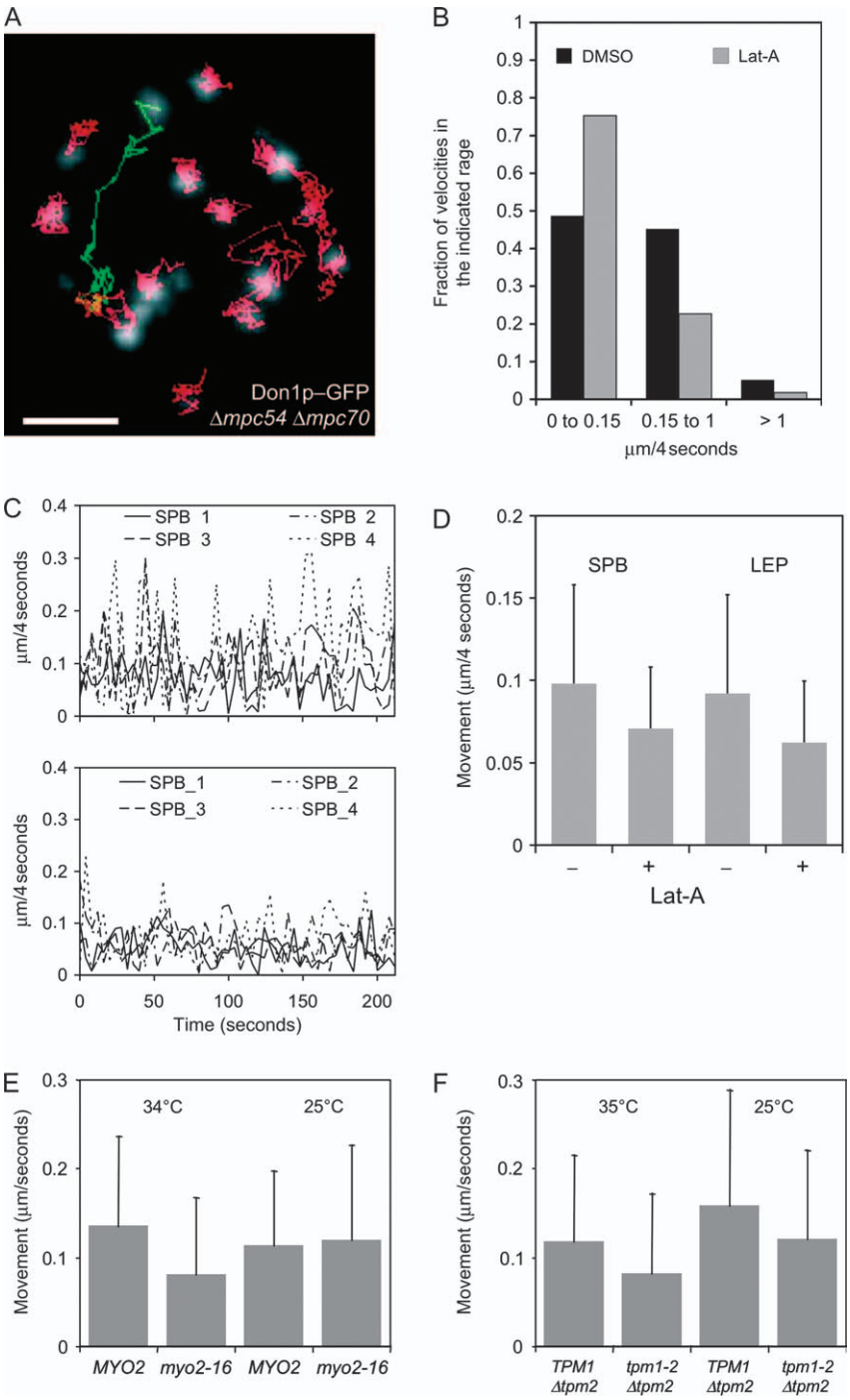

Figure 3: Legend on next page.

indicates that actin cables are not essential for meiosis and spore formation. The *arp2-1* cells formed almost no spores at restrictive temperature. Even at permissive temperature, the sporulation efficiency was much lower than in the control cells.

We followed Don1p–GFP signals in wild-type and *arp2-1* cells at 35°C to see at which stage of sporulation the *arp2-1* cells are defective. This revealed a defect in spore maturation (Figure 5C), similar to the one observed due to Lat-A treatment of wild-type cells (Figure 2C). Ether treatment of wild-type and *arp2-1* cells sporulated at permissive and restrictive temperature confirmed the formation of almost no functional (ether resistant) spores in *arp2-1* cells sporulated at restrictive temperature (Figure 5D). We performed electron microscopy (EM) analysis of *arp2-1* and wild-type cells sporulated at permissive and restrictive temperature. This revealed defects in spore wall assembly in *arp2-1* cells sporulated at 35°C (Figure 5E). The dityrosine layer, which appears in wild-type cells and also in the *arp2-1* at 25°C as a thin black layer around the spores, was not present in the *arp2-1* mutant at 35°C. Instead, black dots were visible around the prospores. The absence of the dityrosine layer was described for mutants defective in the formation of the chitosan layer (17). We performed calcofluor white staining in wild-type and *arp2-1* mutant cells at 25°C and 35°C. We found calcofluor white-stained spore walls in wild-type cells sporulated at both temperatures and in *arp2-1* cells sporulated at 25°C. In contrast, no calcofluor white-stained spore walls could be found in the *arp2-1* mutant cells sporulated at 35°C. Only staining of bud scars was observed (Figure 5F). This indicates a defect in chitosan layer formation in the *arp2-1* mutant. This may prevent the correct formation of the dityrosine layer.

Together, these results indicate that the essential function of Arp2p during spore wall maturation is most likely during the deposition of the chitosan layer. In vegetative cells, the formation of the bud scar, which consists of chitin, requires a specific class of membranous compartments, the so-called chitosomes (31,32).

To address this point more directly, we performed EM on sporulating cells using a fixation and silver staining procedure that allows the visualization of carbohydrate-rich structures (33). This revealed strongly contrasted membranous compartments that appear to be tightly associated with PSMs (Figure 5G). In cells with assembled spore walls, we noticed a thin layer of stained material near the outer side of the spore wall. In these cells, usually no or very few remaining carbohydrate-rich structures were detected (example Figure 5G (iii)). This suggests that these structures contain material that becomes deposited as a continuous layer close to the outside of the spore wall. We next investigated the appearance of these carbohydrate-rich structures in the *arp2-1* mutant. This revealed that their appearance in cells early and during meiosis II was similar to wild type (not shown). In contrast, cells with immature spore walls exhibited often carbohydrate-rich compartments with irregular structures docked to the outside of the spore compartment [Figure 5G (iv)]. In rare cases, we found cells containing spores with a thickened spore wall exhibiting carbohydrate staining at the outside of the spore wall. Several of these asci contained one spore with a thin layer of stained material around the spore wall, whereas the walls of the other spores were devoid of any staining [Figure 5G (v)]. This latter finding is consistent with the observation that the *arp2-1* mutant is still able to form spores at very low frequency.

Together, these results suggest that Arp2p is required for faithful formation of spore walls, and that the specific process affected is related to the biogenesis or transport of membranous compartments. These compartments may transport precursor material of the chitosan layer, and thus be the meiotic equivalent to chitosomes.

Discussion

We have shown that actin plays non-essential and essential roles during sporulation. Furthermore, we investigated

Figure 3: Actin-dependent movements of precursors, SPBs and LEP coats. A) Tracks of precursors recorded over a 2 min period in a *Δmpc54 Δmpc70 DON1–GFP* cell in meiosis II. Frames were taken every 4 seconds. The tracks were superimposed onto the first frame of the movie. The full movie is provided with Movie S5. This movie also shows a walking average processing (of 4 frames), which allows better visualization of the different speeds of the precursors. B) Velocities of all precursor structures measured in cells treated either with DMSO or with DMSO and Lat-A (10 cells each). The movements were categorized according to speeds and shown as fractions of all movements that fall into specific speed ranges. C) Movements of SPBs and LEP coats in cells with (lower graph) and without Lat-A treatment (upper graph). Speeds of the four SPBs from one cell per condition are shown. The velocities were calculated as movements from one frame to the next (μm/4 seconds). Full movies for SPB and LEP coats in treated and untreated cells are provided (Movie S6). D) Quantification of SPB and LEP coat movements in control and Lat-A-treated cells. Recordings from 20 cells for each condition were used for quantification. The standard deviations of the measurements are indicated. E) PSM precursor movements depend on Myo2p. Don1p–GFP signals were recorded in *MYO2* and *myo2-16* cells at permissive (25°C) and restrictive temperatures (34°C) in 1 μm thick sections of the cell (see *Materials and Methods*). The speed of PSM precursor movements was assessed by measuring the distance of PSM precursor movements from one frame to the other using the manual tracker plugin available for ImageJ. F) PSM precursor movements depend on tropomyosin. Measurements in *Δtpm2 TPM1* and *Δtpm2 tpm1-2* cells were done as described in (E) except that the restrictive temperature for *Δtpm2 tpm1-2* was 35°C. The standard deviation of the measured velocities is shown as thin lines. For the experiments with *MYO2*-strains, 3500–4300 vesicle movements were measured per strain and temperature, for *TPM1/2*-strains 1800–4500 vesicle movements. One vesicle movement is the distance a vesicle moves from one frame to the next of a movie.

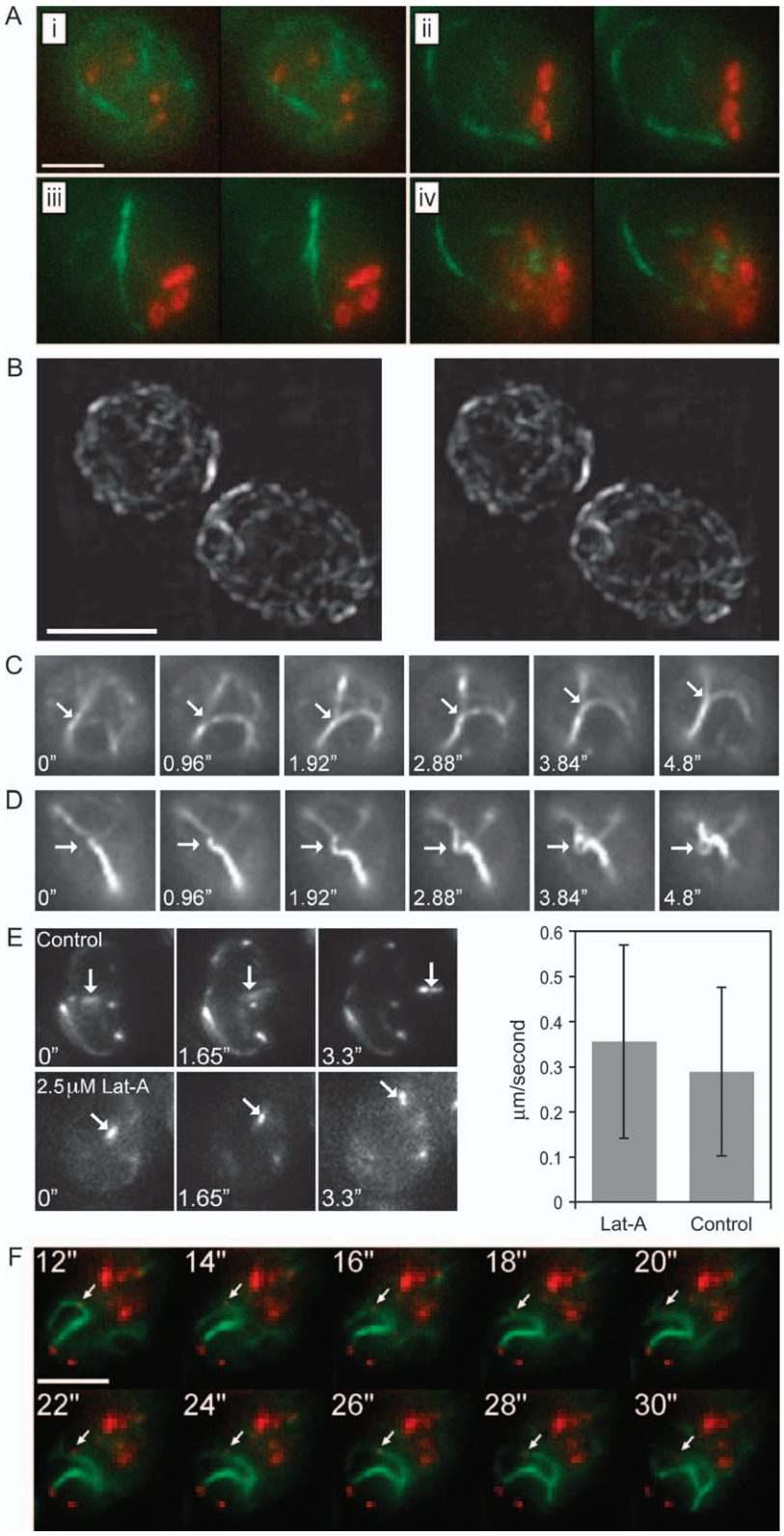

Figure 4: Actin cable organization and dynamics in meiotically dividing cells. A) Time-lapse movie of Abp140p–4GFP- and Don1p–RFP-expressing cells undergoing meiosis and spore formation. Stereo views of 3D reconstructions of selected time-points are shown: (i) cell before PSM formation; (ii) and (iii) cells during PSM growth; (iv) cell after PSM closure. The brightness and contrast was adjusted separately for each picture. (Full movie is provided as Movie S7. In the movie, all adjustments are the same for each frame of the movie.) Bar: 4 μm. B) 3D reconstruction of two cells showing actin cables labelled with Abp140p–4GFP. The picture was reconstructed from a deconvolved image stack taken with a single plane illumination microscope (SPIM) (56). Bar: 4 μm. A movie showing a 360° turn is provided as Movie S8. C) and D). Frames from single planes taken at the periphery of two Abp140p–4GFP cells in meiosis. Full movies provided as Movies S11 and S12. E) Sliding of short actin cables along the plasma membrane in cells in meiosis. The pictures show maximum projections from three frames covering a slice of approximately 1.5-μm thickness. The quantification shows the average and the standard deviation of the speeds of short filaments recorded in the Lat-A and in untreated cells. F) Movement of a Don1p–RFP labelled precursor (arrow) along an actin cable labelled with Abp140p–4GFP. Consecutive frames are shown; numbers indicate time (seconds) after start of the recording of the movie. Bar: 4 μm. The full movie is provided as Movie S13.

the dynamic organization of the actin cytoskeleton during meiosis and spore formation. Previous studies have demonstrated that actin mutants exhibit defects in sporulation (34), and the presence of filamentous actin structures in sporulating yeast cells was observed in fixed cells (25,26). Functional analysis indicated that actin is required for mitochondrion organization (35) as well as for telomere clustering (36) during meiotic prophase. Here, we have

shown that the assembly of the PSMs is associated with Myo2p and tropomyosin-dependent dynamic movements of the PSM precursor structures. Actin cables and patches do not exhibit a polarized organization during sporulation and the role of filamentous actin during PSM assembly is non-essential. This suggests that other processes are responsible for regulating membrane growth and PSM shaping during sporulation. Finally, our studies indicate that spore wall maturation requires functional actin patches because of the failure of an *arp* mutant, but not of tropomyosin mutants, to assemble a normal chitosan and dityrosine layer. Our findings concerning divers roles of filamentous actin during the different steps of meiosis and spore formation are indicated in Figure 6.

Morphogenesis of prospore membranes

Prospore membrane assembly during meiotically dividing cells is equivalent to bud formation in vegetative cells. A number of observations indicate that the morphogenetic processes between the two modes of daughter cell formation are remarkably different. Previous work denoted the essential requirement of the SPB in initiation of the PSM formation (7,11). The PSM assembly occurs separately from the plasma membrane of the mother cell and involves homotypic vesicle fusion and specific regulation of the exocytic machinery (8–10).

Here, we provide several lines of evidence that no polarization of the actin cytoskeleton is required for the formation of spores. First, complete depolymerization of actin using Lat-A does not inhibit the appearance of round prospores (Figure 2C). Second, the selective disruption of actin cables using tropomyosin mutants or actin-cable-based motility of exocytic vesicles in the *myo2-16* mutant does not impair formation of spores (Figure 5B). These results also imply that no contractile acto-myosin ring is required for the closure of the PSMs during post-meiotic cytokinesis. Consistent with this, we could not detect Myo1p or actin at the leading edge of the PSM (data not shown).

Analysis of the dynamics of PSM assembly using Don1p–GFP (7) revealed a contribution of actin-based and Myo2p-dependent movements of PSM precursors. Track analysis revealed that these movements appear not to be directed towards the sites of PSM assembly and growth (Figure 1). This is consistent with the observation that these movements also occur in a mutant with impaired PSM assembly due to the absence of a meiotic SPB component (Figure 3 A). We also observed actin-cable-dependent movements of the SPBs in meiosis II and of the growing PSMs (Figure 3C, D). Together, these observations suggest that actin-cable-dependent movements of the precursors increase the chance of their meeting either the SPBs during the early stages or the growing PSMs. In this respect, actin-dependent mobility would simply enhance the efficient progression through these steps.

We observed also actin-independent movements in all our measurements, which is in accordance with this model and may simply be due to Brownian movement. In addition, the fast, actin-dependent movements of precursors were observed only for a small fraction of the precursors during any given observation period (Figure 1) and only a minority of precursors was found to be associated with actin cables (Figure 4F). The movies (Figure 1A) showing the whole PSM assembly process revealed static precursors as well, which did not move during the whole process of PSM assembly. They faded away concomitantly with the assembly of the LEP coats at the PSMs. It may well be that these structures consist of aggregated LEP coat components which slowly disassemble upon formation of the LEP coats and recruitments of components to these sites.

In general, our model of random movements by actin cables during PSM assembly is in agreement with a model where membrane delivery to the PSM is mediated via non-polarized transport. Actin-based movements might simply lead to a slight acceleration of the process. We measured PSM assembly in single cells and on the level of populations. However, we could not detect a measurable influence of actin cable-based transport on the progression of PSM assembly (Figure 3D). These findings are illustrated on the left side of the model (Figure 6).

Organization of actin cables in meiotically dividing cells

Visualization of actin using a marker that preferentially decorates actin cables in meiosis revealed dynamic filaments that form a cage-like structure at the periphery of the cell (Figure 4A–D). Due to the resolution restriction of light microscopy, we could not determine whether these cables are entirely restricted to the plasma membrane or whether they grow sometimes into the lumen of the cell.

We noticed changes in the appearance of the cables during the course of meiosis and spore formation. Early in meiosis, cells tended to contain many cables, which were weakly fluorescent. Cells in meiosis II showed fewer, but much brighter cables. Usually, only two or three bright cables were present in a cell (Figure 4A, B). This is in agreement with a previous report that actin cables are more prominent during later stages of sporulation (26).

We found that actin cables do interact with each other in different ways. In Figure 4C, frames of a movie are shown in which two actin cables are combined. This resembles very much a zipper and might be due to the cross-linking of actin cables. Figure 4D shows an actin cable that forms a growing loop. It appears that sliding of one cable along another one causes this. The looping out can best be explained by blockage of the tip of the sliding cable and continuous pushing from the tail of the cable. Our analysis thus suggests that at least two different motor proteins

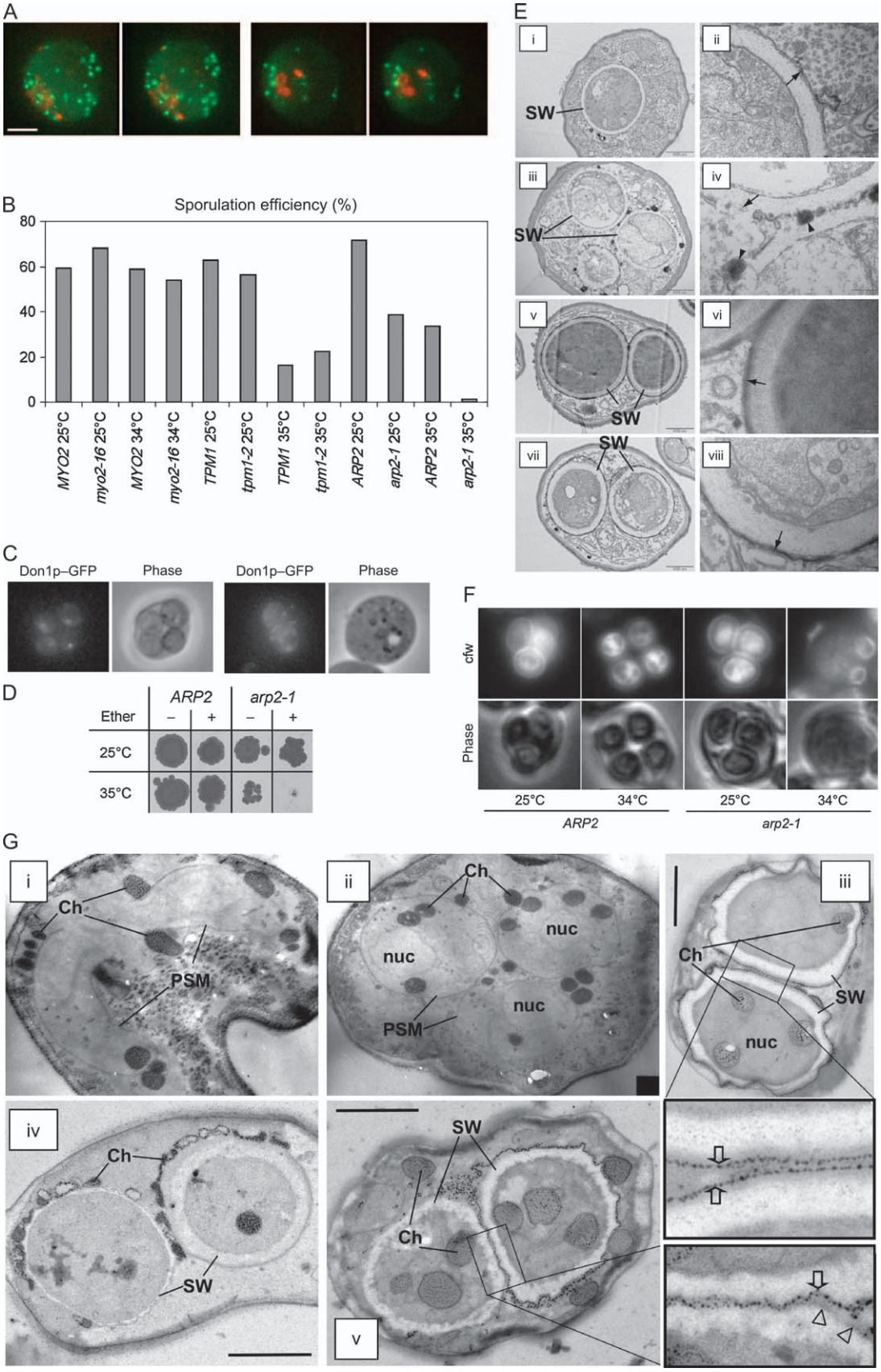

Figure 5: Legend on next page.

may contribute to filament movement: one motor at the plasma membrane required for the sliding of the filaments (Figure 4E) and another motor that allows the sliding of the filaments along each other. It will be interesting in the future to resolve the network of protein–protein interactions and motor proteins that permit the organization of a dynamic cage of actin cables.

Requirement of Arp2p for spore wall maturation

Latrunculin A treatment as well as the *arp2-1* mutant prevented the formation of mature spore walls (Figures 2 C, 5B–F). The Arp2/3p complex constitutes the core of an actin-nucleating activity required for the integrity and mobility of actin patches and branched actin filaments (37). It is required for endocytosis and organelle inheritance (38). The *arp2-1* mutant exhibited a defect at permissive temperature, more pronounced at restrictive temperature, which prevented entry into meiosis in a high fraction of cells (60% showed one nucleus and no duplicated SPBs after 24 h on sporulation medium, data not shown). We observed that the *arp2-1* mutant showed slightly reduced vegetative growth rates (data not shown) and a reduction in sporulation efficiency (Figure 5B) at permissive temperature. This suggests that the mutant is only partially functional at permissive temperature. These results indicate that efficient induction of meiosis and sporulation might require a fully functional actin cytoskeleton. However, all cells that entered meiosis formed PSMs at restrictive temperatures but most of them failed to form mature spore walls (Figure 5B, C). This suggests that Arp2p is not necessary during PSM formation. Another study reported the requirement of End3p during spore wall maturation (26). End3p is a protein involved in endocytosis, cortical actin organization and cell wall morphogenesis in vegetative cells (39). Furthermore, *arp2* and *end3* mutants are synthetically lethal, suggesting their involvement in the same processes (40). Our results are consistent with these studies.

We detected large membranous structures containing cargo with high contents of carbohydrates associated with PSMs (Figure 5G). These compartments may be the meiotic equivalent of chitosomes (41) that transport precursor material for the chitin deposits at the site of cell division in mitotic cells. Chitosome biogenesis and chitin deposition depends on endocytotic machinery (32), which also requires the function of actin (42). It may thus be that the meiotic equivalents of chitosomes are required for the formation of the chitosan layer of the PSM (15), which only becomes deposited once the PSM has been closed (17). Therefore, the observation of the failure in spore wall maturation in Lat-A-treated cells and in the *arp2-1* mutant is consistent with a defect in chitosome biogenesis as a cause for the absent chitosan layer (Figure 5F). This is qualitatively confirmed by our EM data where we used a silver staining procedure that allows the detection of carbohydrate-rich structures (Figure 5G). These data, however, reveal the presence of carbohydrate-rich compartments, presumably chitosomes, also in the *arp2-1* mutant, and a defect associated with later stages, deposition of the content of the compartments in the spore wall. The observation that in these cases the dityrosine layer is also defective (Figure 5D, E) is consistent with the previous finding that the chitosan layer is needed for proper formation of the outermost dityrosine layer of the spore wall (17). These findings support the idea that the silver staining procedure specifically detects the chitosan layer, and that the large membranous carbohydrate-rich compartments are in fact chitosomes. An essential requirement of chitosomes in spore wall deposition also explains the previous notion that in the *Δend3* mutant, chitin synthase III fails to localize to the spore wall (26).

Actin was also found to be non-essential for another type of intracellular daughter cell formation (intracellular budding) during endodyogeny in the protist *Toxoplasma gondii* (43). Protist intracellular budding resembles in many other respects the processes of PSM formation (44). In this instance, the inner membrane complex (IMC) is assembled in close vicinity to the centrosomes, and a specific type of microtubule organizing centre, the conoid, is an integral part of the assembled IMC (45,46).

Figure 5: Arp2p, but not tropomyosin is required for spore wall formation. A) Time-lapse movie of GFP–Cap2p- and Don1p–RFP-expressing cells undergoing meiosis. Stereo views of 3D reconstructions of two selected time-points are shown: (i) cell before PSM formation; (ii) cell during PSM growth. The full movies are provided as Movies S14 and S15. Bar: 4 μm. B) *MYO2* and *myo2-16* cells were sporulated at permissive (25°C) or restrictive temperature (34°C). *Δtpm2 TPM1, Δtpm2 tpm1-2, ARP2* and *arp2-1* cells were sporulated at permissive (25°C) or restrictive temperature (35°C). Sporulation efficiency was assessed after 36 h. C) Don1p–GFP fluorescence and phase contrast images from *arp1-2* and corresponding wild-type cells sporulated at 35°C for 8 h. D) Ether test performed with wild-type and *arp2-1* mutant cells sporulated at 25°C and 35°C. Equal number of cells were spotted on plates followed by ether treatment as indicated. E) Electron microscopy of sporulated wild-type and *arp2-1* mutant cells. (i) wild-type cell sporulated at 35°C; (iii) *arp2-1* cell sporulated at 35°C; (v) wild-type cell sporulated at 25°C; (vii) *arp2-1* cell sporulated at 25°C. (ii), (iv), (vi) and (viii): higher magnification of the cells shown in (i), (iii), (v) and (vii). Bar size is 1000 nm for the panels (i), (iii), (v) and (vii) and 200 nm for the panels (ii), (iv), (vi) and (viii). F) Calcofluor staining of sporulated wild-type and *arp2-1* mutant cells. The arrows point to the stained bud scars in the *arp2-1* mutant sporulated at restrictive temperature. G) Visualization of large carbohydrate containing organelles in wild-type and *arp2-1* mutant cells sporulated at 30°C (i and ii) or 34°C (iii–v) using EM and a staining procedure specific for carbohydrates (see *Material and Methods*). Wild type, i–iii; *arp2-1*, iv and v. Three wild-type cells, one in meiosis II (i), one after completion of meiosis II (ii) and one after spore wall assembly (iii) are shown. nuc, nucleus; Ch, chitosome-like structure; SW, spore wall. Arrows in the enlarged sections denote spore walls, which exhibit silver staining of the outermost layer. Arrow heads point to a layer that is devoid of the silver staining.

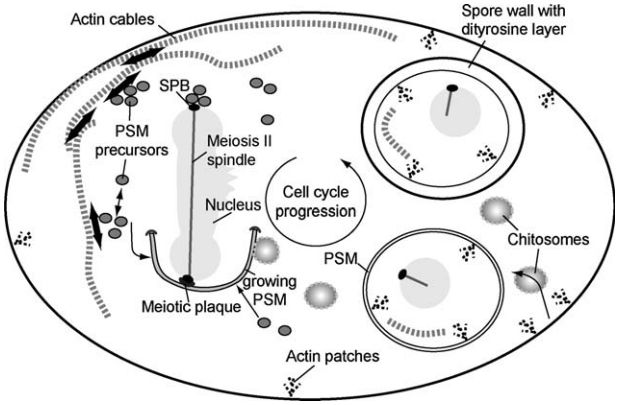

Figure 6: Model of actin-based processes during yeast meiosis and spore formation. The different roles of actin, as revealed in this study, are shown at different cell cycle stages. Situations early in meiosis II (before initiation of PSM assembly, top left), during meiosis II (growing PSM, bottom left), after PSM closure (inmature prospore, bottom right) and after completion of spore wall assembly (mature spore, top right) are shown.

Materials and Methods

Yeast strains, plasmids, growth media and growth conditions

Basic yeast methods and growth media were as described (47). All strains used for this study were derivatives of the SK-1 strains YKS32 or LH177. All yeast strains we generated during this study are listed in Table 1. The plasmids pRS306-*MYO2,* pRS306-*myo2-16,* pRS314-*TPM1* and pRS314-*tpm1-2* (23) were kind gifts of D. Pruyne and A. Bretscher. To generate the *MYO2* (YCT977) and *myo2-16* (YCT978) strains, the plasmids pRS306-*MYO2* and pRS306-*myo2-16* were cut with *Spe*I and transformed into yeast cells. Chromosomal manipulations of yeast strains (gene deletions and C-terminal gene tagging) were performed using polymerase chain reaction (PCR)-amplified cassettes as described (48–50). The homozygous diploid *ABP140–4GFP* (YCT791) strain was constructed using PCR-based tagging of *ABP140* by using plasmid pSM1023 (51) in haploid cells prior to diploidization. The plasmids pFA6a-tdimer2-kanMX6 and pFA6a-tdTomato-natNT2 were used to generate the Don1p–RFP strains (YCT1035 and YCT974). Both plasmids were constructed as previously described for other pFA6a plasmids (48). The *tdTomato* gene was constructed using full gene synthesis (52) with a codon usage adapted for expression in yeast. The fluorescence properties of *tdimer2* and *tdTomato* are described elsewhere (53). Polymerase chain reaction and immunoblotting were used to verify the correct integration of the cassettes. Synchronous sporulation was performed using the pre-growth regimes from Alani *et al.* (54). Potassium acetate (0.3%) was used as sporulation medium. Hoechst 33342 staining upon fixation with 70% ethanol was performed routinely to monitor progression through meiosis and sporulation. The ether vapour treatment was done as described (55).

Lat-A treatment

Latrunculin A treatment was performed as described (21). A concentration of 0.2 mM was used to depolymerize actin filaments completely. Filamentous actin depolymerization by Lat-A was verified using phalloidin labelling or GFP–Cap2p and Apb140p–4GFP cells. To ensure that Lat-A was present in excess during long-time incubations, we added the medium after completion of the experiment to GFP–Cap2p Abp140p–4GFP cells and verified on the microscope that it contained still enough Lat-A to completely depolymerize GFP-labelled actin structures. For the experiment shown in Figure 4E, an optimal concentration of 2.5 μM was empirically determined for sporulating cells. This concentration depolymerizes actin in sporulating cells completely after an incubation period of 20–40 min. The experiment was performed as soon as an increased number of short actin cables became visible (after approximately 10-min incubation time).

Table 1: Yeast strains used in this study

Name	Genotype	Source
YKS32	*Mat***a***/Matα ura3/ura3 lys2/lys2 ho::hisG/ho::LYS2 leu2::hisG/LEU2*	(7)
LH177	*Mat***a***/Matα ho::hisG/ho::hisG lys2/lys2 ura3/ura3 leu2/leu2 his3/his3 trp1ΔFA/trp1ΔFA*	(58)
YKS53	YKS32 *DON1::GFP::kanMX/DON1::GFP::kanMX*	(7)
YKS65	YKS53 *Δmpc54::kanMX/Δmpc54::kanMX Δmpc70::kanMX/Δmpc70::kanMX*	(7)
YCT977	YKS53 *MYO2::URA3/MYO2::URA3*	This study
YCT978	YKS53 *myo2-16::URA3/myo2-16::URA3*	This study
YCT1022	LH177 *DON1::GFP::kanMX/DON1::GFP::kanMX Δtpm1::natNT/Δtpm1::natNT2 Δtpm2::hphNT1/Δtpm2::hphNT1* pRS314-*TPM1*	This study
YCT1023	LH177 *DON1::GFP::kanMX/DON1::GFP::kanMX Δtpm1::natNT2/Δtpm1::natNT2 Δtpm2::hphNT1/Δtpm2::hphNT1* pRS314-*tpm1-2*	This study
YCT791	YKS32 *ABP140::4GFP::kanMX/ABP140::4GFP::kanMX*	This study
YCT1035	YCT791 *DON1::tdtomato::natNT2/DON1::tdtomato::natNT2*	This study
YCT1043	YCT1035 *Δmpc54::hphNT1/Δmpc54::hphNT1*	This study
YCT974	YKS32 *cap2::URA3::GFP::CAP2/cap2::URA3::GFP::CAP2 DON1::tdimer2::kanMX/DON1::tdimer2::kanMX*	This study
YCT1058	YKS53 *arp2-1::URA3/arp2-1::URA3*	This study

Microscopy

Live cell imaging

Sporulating cells (0.2 mL) were adsorbed on coated (Concanavalin A, 6% in water) glass-bottomed small Petri dishes (MaTek Corporation, Ashland, MA, USA) for 20 min, washed twice with sporulation medium and observed under an inverted epifluorescence microscope (Leica DM-IRBE; Leica Microsystems GmbH, Wetzlar, Germany) using a 63× oil lens (NA 1.4). This treatment did not affect sporulation efficiency, if the cells were allowed to complete sporulation in a humid chamber. METAMORPH™ software, a Coolsnap HQ camera (Photometrics, Roper Scientific GmbH, Ottobrunn, Germany) and a piezo stepper were used to acquire z-stacks with a distance of 0.6 μm between the single planes. The pictures of one z-stack were combined into a single frame using maximum projections. Live cell imaging (Figures 3E, F, 4A, F and 5A) was performed on a DeltaVision Spectris (AppliedPrecision, LLC, Issaquah, WA, USA) equipped with GFP and Cy3 filters, a 100× oil immersion objective with a numerical aperture of 1.4, SOFTWORX™ software and CoolSnap HQ camera. The z-stacks were recorded with a distance of 0.6 μm between single planes. The point and object tracking functions of METAMORPH™ software were used to record velocities of PSM precursors and LEP coats (Figures 1C and 3).

METAMORPH™ was also used to generate the plots shown in Figure 3C. The manual tracker plugin available for ImageJ was used to measure PSM precursor movements (Figure 3E, F). The z-sweep acquisition (OAI™) function of the DELTAVISION SPECTRIS SOFTWORX™ acquisition software was used with a movement of 1 μm to record the images (measurements shown in Figure 3E, F). The walking average movie was generated with ImageJ (walking average plugin) as follows: The first frame of the walking average is a projection of the images 1–4. The second frame is a projection of the images 2–5, the third frame uses the images 3–6 and so on. Data analysis was performed using electronic spreadsheet software.

EM

For the pictures of Figure 5G, silverproteinate contrasting of carbohydrates of Araldite (Sigma-Aldrich, St. Louis, USA) embedded cells was performed as described (33). For Figure 5E, potassium permanganate fixation was done as described (7). The images were collected with a Morgani 268D (FEI Company, Hillsboro, Oregon, USA) electron microscope equipped with a Megaview III camera (Soft Imaging System, Münster, Germany).

Single plane illumination microscopy

Yeast cells embedded in 0.5% low melting point agarose inside a capillary (1-mm diameter) were transferred to the microscope 4 h after induction of sporulation. A solution of 0.1% potassium acetate in water was used as incubation medium. Single plane illumination microscopy (SPIM) setup was as described (56). We used an Achroplan 100× water immersion lens (NA 1.0) and a Hamamatsu Orca-ER CCD camera (Hamamatsu Photonics Deutschland GmbH, Herrsching, Germany) for the imaging. The cells were kept in 0.1% potassium acetate solution during the data acquisition. The cells completed sporulation under these conditions within 24 h (data not shown).

Calcofluor white staining

Staining was done as described (57). Briefly, the cells were sporulated in 0.3% potassium acetate for 24 h and then treated with 70% ethanol for 1 h. The cells were collected by centrifugation, washed once with water, incubated for 5 min with 100 μL fluorescence brightener 28 (1 mg/mL; Sigma-Aldrich, St. Louis, MO, USA), washed again with water and visualized under the microscope (Leica RXA, 100× oil lens, NA 1.4; Leica MicrosystemsGmbH) using a DAPI filter set and a photometrics CoolSnap cf CCD camera (Photometrics, Roper Scientific, GmbH).

Actin staining with phalloidin–Alexa$_{583}$

Sporulating or mitotically dividing cells were fixed in PM buffer (100 mM potassium phosphate pH 6.8, 2 mM $MgSO_4$) with 3% formaldehyde at room temperature for 1 h. After three washing steps with PM buffer, the cells were resuspended in 1 mL PM containing 1% Triton-X-100 and incubated at room temperature for 3 min to allow cell permeabilization. Permeabilized cells were washed with PM buffer, resuspended in 100 μL phalloidin–Alexa$_{583}$ (1/100 dilution; Molecular Probes Inc., Eugene, OR, USA)/PM buffer and incubated at room temperature for 1 h. Hoechst 33342 was added (1 μM end concentration) to the cells. The cells were mounted on a glass slide and immediately transferred to the microscope. A DeltaVision Spectris (AppliedPrecision, LLC) equipped with DAPI and Cy3 filter sets, a 100× oil immersion lens (NA 1.4), SOFTWORX™ software and CoolSnap HQ camera (Photometrics, Roper Scientific, GmbH) was used to collect image stacks with 0.6-μm distance between single planes. The z-projections were done using the Quick projection tool of SOFTWORX™ (maximum projections).

Acknowledgments

We are grateful to M. Matzner, K. Goldie, Uta Haselmann-Weiß and N. Ly-Hartig for help with electron microscopes, T. Zimmermann, S. Terjung and J. Rietdorf for help with light microscopes. D. Pruyne and A. Bretscher are kindly acknowledged for the *myo2* and *tpm1* mutant plasmids. J. Schaletzky is kindly acknowledged for additional help and D. DiToro for critical reading of the manuscript. C.T., E.H.K.S. and M.K. received support from the ''Forschung Optische Technologien 2003/2004'' research program of the ''Landesstiftung Baden-Württemberg gGmbH''.

Supplementary Materials

Figure S1: Actin organization in mitotic and meiotic cells in wild-type and Abp140p–4GFP cells. Actin was visualized using rhodamine–phalloidin, DNA using Hoechst 33342 staining. The size of the bar is 4 μm. (i) wild-type cell during mitotic cell division. (ii) *ABP140::4GFP* cell during mitotic cell division. (iii) wild-type cell during meiosis I. (iv) *ABP140::4GFP* cell during meiosis I. (v) wild-type cell during meiosis II. (vi) *ABP140::4GFP* cell during meiosis II.

Movie S1: The movie shows a Don1p–GFP-expressing cell undergoing PSM assembly. Maximum projections from image stacks taken every minute are used for the assembly of the movie. The movie corresponds to the frames from Figure 1A. Movie plays at one frame per 0.1 second.

Movie S2: The movie shows a Don1p–GFP-expressing cell undergoing PSM growth and closure. Movie recording conditions as for Movie S1. The movie corresponds to the frames from Figure 1B. Movie plays at one frame per 0.1 second.

Movie S3: The movie shows a Don1p–GFP-expressing cell in meiosis during the time-point of PSM assembly. Maximum projections from image stacks taken every 4 seconds are used for the assembly of the movie. The first frame of the movie shows two arrows pointing to the two precursor structures, for which merging was observed (Figure 1C). Movie plays at one frame per 0.1 second.

Movie S4: As for Movie S3, but for the cell shown in Figure 1D.

Movie S5: Precursor movement in *Δmpc54 Δmpc70*- and Don1p–GFP-expressing cells in meiosis. Recording conditions as for Movie S3. To the right of the movie is a processed version using a walking average of four frames. This movie was generated using ImageJ and the walking average plugin. This allows better visualization of fast movements. The movie corresponds to Figure 3A.

Movie S6: The movie shows a montage of four cells from two different stages of PSM assembly. In the cells in an early phase (two cells on the top), the Don1p–GFP staining is associated with precursors in the cytoplasm and at the SPBs (indicated). The four SPBs can easily be distinguished from other precursors, because they move in a pair wise manner, which is due to the two short meiosis II spindle that connect them in pairs. In later stages (cells at the bottom), Don1p–GFP localizes to the LEP coat (indicated). Control cells (two cells to the left) and Lat-A-treated cells are shown. The movie corresponds to Figure 3C and D.

Movie S7: Time-lapse movie of Abp140p–4GFP and Don1p–RFP expressing cells undergoing meiosis. The movie shows 12 time-points during meiosis, each represented by a full turn of the cell. The data stacks were recorded every 15 min. Each turn was created from projections (10° intervals) using SOFTWORX™ of a data stack recorded at the respective time-point. Don1p–RFP (red colour) labelled PSM precursors, LEP coats (donut stage) and diffuse Don1p–RFP staining (after closure of the PSMs) and actin cables (Abp140–4GFP, green colour) can be identified. The movie corresponds to Figure 5A.

Movie S8: Actin cable organization in meiosis. The movie shows a 360° surround view of two Abp140–4GFP-expressing cells during meiosis. The

data stack was recorded using a SPIM (56) and deconvolved. Projections were created every 5° using ImageJ. The movie corresponds to Figure 5B.

Movie S9 and S10: Visualization of actin cable dynamics in meiosis using Abp140p–4GFP cells. The movie shows a single plane from the periphery of a cell. Pictures were taken every 96 milliseconds. The movie corresponds to Figure 5C and D.

Movie S11: Movement of a short actin cable. Movie shows maximum projections from three planes recorded from the periphery of a cell spanning a section of approximately 1.5 μm. Frames were taken every 820 milliseconds. The movie corresponds to Figure 5E.

Movie S12: Movement of a short actin cable in a cell treated with a low dose of Lat-A. Movie recording as for Movie S11. The movie corresponds to Figure 5E.

Movie S13: Movement of a Don1p–RFP (red colour) labelled precursor along an actin cable in a *Δmpc54* cell in meiosis II. The actin cable was visualized using Abp140p–4GFP (green colour). The frames were taken every 2 seconds. The movie corresponds to Figure 5F.

Movie S14: Time-lapse movie of GFP–Cap2p- and Don1p–RFP-expressing cells undergoing meiosis. The movie shows 12 time-points during meiosis, each represented by a full turn of the cell. The data stacks were recorded every 15 min. Each turn was created from projections (10° intervals) of a data stack recorded at the respective time-point. Don1p–RFP (red colour) labelled PSM precursors, LEP coats (donut stage) and actin patches (GFP–Cap2p, green colour) can be identified. The transition from precursor to donut stage is shown. The movie corresponds to Figure 6A (i) and (ii).

Movie S15: Same as Movie S14, but the transition from donut stage to closed PSM is shown.

Supplemental materials are available as part of the online article at http://www.blackwell-synergy.com

References

1. Pruyne D, Bretscher A. Polarization of cell growth in yeast. J Cell Sci 2000;113:571–585.
2. Bretscher A. Polarized growth and organelle segregation in yeast: the tracks, motors, and receptors. J Cell Biol 2003;160:811–816.
3. Moreno-Borchart AC, Knop M. Prospore membrane formation: how budding yeast gets shaped in meiosis. Microbiol Res 2003;158:83–90.
4. Peterson JB, Gray RH, Ris H. Meiotic spindle plaques in Saccharomyces cerevisiae. J Cell Biol 1972;53:837–841.
5. Zickler D, Olson LW. The synaptonemal complex and the spindle plaque during meiosis in yeast. Chromosoma 1975;50:1–23.
6. Davidow LS, Goetsch L, Byers B. Preferential occurrence of nonsister spores in two-spored asci of *Saccharomyces cerevisiae*: evidence for regulation of spore-wall formation by the spindle pole body. Genetics 1980;94:581–595.
7. Knop M, Strasser K. Role of the spindle pole body of yeast in mediating assembly of the prospore membrane during meiosis. EMBO J 2000;19:3657–3667.
8. Knop M, Miller KJ, Mazza M, Feng D, Weber M, Keranen S, Jantti J. Molecular interactions position Mso1p, a novel PTB domain homologue, in the interface of the exocyst complex and the exocytic SNARE machinery in yeast. Mol Biol Cell 2005;16:4543–4556.
9. Riedel CG, Mazza M, Maier P, Korner R, Knop M. Differential requirement for phospholipase D/SPO14 and its novel interactor SMA1 for regulation of exocytotic vesicle fusion in yeast meiosis. J Biol Chem 2005;280:37846–37852.
10. Neiman AM. Prospore membrane formation defines a developmentally regulated branch of the secretory pathway in yeast. J Cell Biol 1998;140:29–37.
11. Bajgier BK, Malzone M, Nickas M, Neiman AM. SPO21 is required for meiosis-specific modification of the spindle pole body in yeast. Mol Biol Cell 2001;12:1611–1621.
12. Nickas ME, Schwartz C, Neiman AM. Ady4p and Spo74p are components of the meiotic spindle pole body that promote growth of the prospore membrane in Saccharomyces cerevisiae. Eukaryot Cell 2003;2:431–445.
13. Moreno-Borchart AC, Strasser K, Finkbeiner MG, Shevchenko A, Knop M. Prospore membrane formation linked to the leading edge protein (LEP) coat assembly. EMBO J 2001;20:6946–6957.
14. Nickas ME, Neiman AM. Ady3p links spindle pole body function to spore wall synthesis in Saccharomyces cerevisiae. Genetics 2002;160:1439–1450.
15. Briza P, Ellinger A, Winkler G, Breitenbach M. Chemical composition of the yeast ascospore wall. The second outer layer consists of chitosan. J Biol Chem 1988;263:11569–11574.
16. Briza P, Winkler G, Kalchhauser H, Breitenbach M. Dityrosine is a prominent component of the yeast ascospore wall. A proof of its structure. J Biol Chem 1986;261:4288–4294.
17. Coluccio A, Bogengruber E, Conrad MN, Dresser ME, Briza P, Neiman AM. Morphogenetic pathway of spore wall assembly in Saccharomyces cerevisiae. Eukaryot Cell 2004;3:1464–1475.
18. Lynn RR, Magee PT. Development of the spore wall during ascospore formation in Saccharomyces cerevisiae. J Cell Biol 1970;44:688–692.
19. Winter D, Podtelejnikov AV, Mann M, Li R. The complex containing actin-related proteins Arp2 and Arp3 is required for the motility and integrity of yeast actin patches. Curr Biol 1997;7:519–529.
20. Pruyne D, Bretscher A. Polarization of cell growth in yeast. I. Establishment and maintenance of polarity states. J Cell Sci 2000;113:365–375.
21. Ayscough KR, Stryker J, Pokala N, Sanders M, Crews P, Drubin DG. High rates of actin filament turnover in budding yeast and roles for actin in establishment and maintenance of cell polarity revealed using the actin inhibitor latrunculin-A. J Cell Biol 1997;137:399–416.
22. Schott DH, Collins RN, Bretscher A. Secretory vesicle transport velocity in living cells depends on the myosin-V lever arm length. J Cell Biol 2002;156:35–39.
23. Pruyne DW, Schott DH, Bretscher A. Tropomyosin-containing actin cables direct the Myo2p-dependent polarized delivery of secretory vesicles in budding yeast. J Cell Biol 1998;143:1931–1945.
24. Zar JH. Biostatistical Analysis. 4th edn. Upper Saddle River, NJ: Prentice-Hall, Inc.; 1999.
25. Doyle T, Botstein D. Movement of yeast cortical actin cytoskeleton visualized in vivo. Proc Natl Acad Sci U S A 1996;93:3886–3891.
26. Morishita M, Engebrecht J. End3p-mediated endocytosis is required for spore wall formation in Saccharomyces cerevisiae. Genetics 2005;170:1561–1574.
27. Asakura T, Sasaki T, Nagano F, Satoh A, Obaishi H, Nishioka H, Imamura H, Hotta K, Tanaka K, Nakanishi H, Takai Y. Isolation and characterization of a novel actin filament-binding protein from Saccharomyces cerevisiae. Oncogene 1998;16:121–130.
28. Yang HC, Pon LA. Actin cable dynamics in budding yeast. Proc Natl Acad Sci U S A 2002;99:751–756.

29. Byers B, Goetsch L. Reversible pachytene arrest of Saccharomyces cerevisiae at elevated temperature. Mol Gen Genet 1982;187: 47–53.
30. Madania A, Dumoulin P, Grava S, Kitamoto H, Scharer-Brodbeck C, Soulard A, Moreau V, Winsor B. The Saccharomyces cerevisiae homologue of human Wiskott-Aldrich syndrome protein Las17p interacts with the Arp2/3 complex. Mol Biol Cell 1999;10:3521–3538.
31. Chuang JS, Schekman RW. Differential trafficking and timed localization of two chitin synthase proteins, Chs2p and Chs3p. J Cell Biol 1996;135:597–610.
32. Ziman M, Chuang JS, Schekman RW. Chs1p and Chs3p, two proteins involved in chitin synthesis, populate a compartment of the Saccharomyces cerevisiae endocytic pathway. Mol Biol Cell 1996;7: 1909–1919.
33. Breton AM, Schaeffer J, Aigle M. The yeast Rvs161 and Rvs167 proteins are involved in secretory vesicles targeting the plasma membrane and in cell integrity. Yeast 2001;18:1053–1068.
34. Whitacre J, Davis D, Toenjes K, Brower S, Adams A. Generation of an isogenic collection of yeast actin mutants and identification of three interrelated phenotypes. Genetics 2001;157:533–543.
35. Smith MG, Simon VR, O'Sullivan H, Pon LA. Organelle-cytoskeletal interactions: actin mutations inhibit meiosis-dependent mitochondrial rearrangement in the budding yeast Saccharomyces cerevisiae. Mol Biol Cell 1995;6:1381–1396.
36. Trelles-Sticken E, Adelfalk C, Loidl J, Scherthan H. Meiotic telomere clustering requires actin for its formation and cohesin for its resolution. J Cell Biol 2005;170:213–223.
37. Machesky LM, Gould KL. The Arp2/3 complex: a multifunctional actin organizer. Curr Opin Cell Biol 1999;11:117–121.
38. Goode BL, Rodal AA. Modular complexes that regulate actin assembly in budding yeast. Curr Opin Microbiol 2001;4:703–712.
39. Tang HY, Xu J, Cai M. Pan1p, End3p, and S1a1p, three yeast proteins required for normal cortical actin cytoskeleton organization, associate with each other and play essential roles in cell wall morphogenesis. Mol Cell Biol 2000;20:12–25.
40. Moreau V, Galan JM, Devilliers G, Haguenauer-Tsapis R, Winsor B. The yeast actin-related protein Arp2p is required for the internalization step of endocytosis. Mol Biol Cell 1997;8:1361–1375.
41. Schekman R, Brawley V. Localized deposition of chitin on the yeast-cell surface in response to mating pheromone. Proc Natl Acad Sci U S A 1979;76:645–649.
42. Riezman H, Munn A, Geli MI, Hicke L. Actin-, myosin- and ubiquitin-dependent endocytosis. Experientia 1996;52:1033–1041.
43. Shaw MK, Compton HL, Roos DS, Tilney LG. Microtubules, but not actin filaments, drive daughter cell budding and cell division in Toxoplasma gondii. J Cell Sci 2000;113:1241–1254.
44. Taxis C, Knop M. Regulation of exocytotic events by centrosome-analogues structures. Topics Curr Genet 2004;10:193–207.
45. Morrissette NS, Sibley LD. Cytoskeleton of apicomplexan parasites. Microbiol Mol Biol Rev 2002;66:21–38.
46. Striepen B, Crawford MJ, Shaw MK, Tilney LG, Seeber F, Roos DS. The plastid of Toxoplasma gondii is divided by association with the centrosomes. J Cell Biol 2000;151:1423–1434.
47. Sherman F. Getting started with yeast. Methods Enzymol 1991;194: 3–121.
48. Janke C, Magiera MM, Rathfelder N, Taxis C, Reber S, Maekawa H, Moreno-Borchart A, Doenges G, Schwob E, Schiebel E, Knop M. A versatile toolbox for PCR-based tagging of yeast genes: new fluorescent proteins, more markers and promoter substitution cassettes. Yeast 2004;21:947–962.
49. Knop M, Siegers K, Pereira G, Zachariae W, Winsor B, Nasmyth K, Schiebel E. Epitope tagging of yeast genes using a PCR-based strategy: more tags and improved practical routines. Yeast 1999;15:963–972.
50. Wach A, Brachat A, Pohlmann R, Philippsen P. New heterologous modules for classical or PCR-based gene disruptions in Saccharomyces cerevisiae. Yeast 1994;10:1793–1808.
51. Maekawa H, Usui T, Knop M, Schiebel E. Yeast Cdk1 translocates to the plus end of cytoplasmic microtubules to regulate bud cortex interactions. EMBO J 2003;22:438–449.
52. Knop M, Barr F, Riedel CG, Heckel T, Reichel C. Improved version of the red fluorescent protein (drFP583/DsRed/RFP). Biotechniques 2002;33:592, 594, 596–598 passim.
53. Shaner NC, Campbell RE, Steinbach PA, Giepmans BN, Palmer AE, Tsien RY. Improved monomeric red, orange and yellow fluorescent proteins derived from Discosoma sp. red fluorescent protein. Nat Biotechnol 2004;22:1567–1572.
54. Alani E, Padmore R, Kleckner N. Analysis of wild-type and rad50 mutants of yeast suggests an intimate relationship between meiotic chromosome synapsis and recombination. Cell 1990;61:419–436.
55. Rockmill B, Lambie EJ, Roeder GS. Spore enrichment. Methods Enzymol 1991;194:146–149.
56. Huisken J, Swoger J, Del Bene F, Wittbrodt J, Stelzer EH. Optical sectioning deep inside live embryos by selective plane illumination microscopy. Science 2004;305:1007–1009.
57. Pringle JR. Staining of bud scars and other cell wall chitin with calcofluor. Methods Enzymol 1991;194:732–735.
58. Huang LS, Doherty HK, Herskowitz I. The Smk1p MAP kinase negatively regulates Gsc2p, a 1,3-beta-glucan synthase, during spore wall morphogenesis in Saccharomyces cerevisiae. Proc Natl Acad Sci U S A 2005;102:12431–12436.